n-alkanes on MgO(100). I. Coverage-dependent desorption kinetics of *n*-butane

Steven L. Tait
Department of Physics, University of Washington, Seattle, Washington 98195-1560

Zdenek Dohnálek
Chemical Sciences Division, Fundamental Sciences Directorate, Pacific Northwest National Laboratory, Richland, Washington 99352

Charles T. Campbell
Department of Chemistry, University of Washington, Seattle, Washington 98195-1700

Bruce D. Kay[a)]
Chemical Sciences Division, Fundamental Sciences Directorate, Pacific Northwest National Laboratory, Richland, Washington 99352

(Received 25 October 2004; accepted 8 February 2005; published online 27 April 2005)

High-quality temperature-programmed desorption (TPD) measurements of *n*-butane from MgO(100) have been made for a large number of initial butane coverages (0–3.70 ML, ML–monolayers) and a wide range of heating ramp rates (0.3–10 K/s). We present a TPD analysis technique which allows the coverage-dependent desorption energy to be accurately determined by mathematical inversion of a TPD spectrum, assuming only that the preexponential factor (prefactor) is coverage independent. A variational method is used to determine the prefactor that minimizes the difference between a set of simulated TPD spectra and corresponding experimental data. The best fit for butane desorption from MgO is obtained with a prefactor of $10^{15.7\pm1.6}$ s^{-1}. The desorption energy is 34.9 ± 3.4 kJ/mol at 0.5-ML coverage, and varies with coverage approximately as $E_d(\theta)=34.5+0.566\theta+8.37\exp(-\theta/0.101)$. Simulations based on these results can accurately reproduce TPD experiments for submonolayer initial coverages over a wide range of heating ramp rates (0.3–10 K/s). Advantages and limitations of this method are discussed. © *2005 American Institute of Physics*. [DOI: 10.1063/1.1883629]

INTRODUCTION

Alkane adsorption on oxide surfaces is of significant interest because of the wide use of oxides in heterogeneous catalysts as support materials and as active catalysts. For example, MgO catalysts are used for the oxidative coupling of methane to form C_2 hydrocarbons or for methane oxidation to produce formaldehyde.[1,2] The MgO(100) surface is one of the most thoroughly studied of all single-crystal oxide surfaces from both experimental and theoretical approaches[3,4] and has also received significant attention as a support in model catalyst studies.[5–7] Therefore, the adsorption and desorption kinetics of alkane molecules on MgO and other oxide surfaces is of fundamental interest. Previous studies addressed the desorption of butane from metal surfaces such as Cu(111),[8] Pt(111),[8–10] Ru(001),[11] and Au(111).[12] Few studies have been conducted on oxide surfaces; we note that Slayton *et al.*[13] studied desorption of butane, hexane, and octane on aluminum oxide. Using Redhead peak temperature analysis and the variation of heating rate method, they obtained a desorption activation energy for butane from Al_2O_3(0001) of 35.1 ± 5.9 kJ/mol with a preexponential factor (prefactor) of $4\times10^{10\pm2.5}$ s^{-1}. Their data suggest that the relative magnitude of molecule-surface interactions compared to molecule–molecule interactions decreases with increasing alkane chain length.[13]

The desorption kinetics can yield significant information about the energy barrier to desorption and prefactor in the desorption rate equation. Recent studies of larger alkane molecules (C_NH_{2N+2}, $N=5-60$) have elucidated their desorption kinetics on graphite.[14–16] These results show a nonlinear dependence of desorption energy on chain length due to partial detachment conformational entropy,[14] which is not expected to play a significant role for the small alkanes. Experiments for small alkanes ($N<5$) have been elusive because of the low sample temperatures required for their adsorption.

This paper is the first in a two-article series regarding the desorption of small alkanes from MgO(100). In the present paper, we discuss the desorption kinetics of butane from MgO(100). We introduce a method to obtain coverage-dependent kinetic parameters from TPD experiments. We assume a coverage-independent prefactor and mathematically invert a TPD spectrum to obtain a coverage-dependent desorption energy. These data are used to simulate a set of TPD spectra with varying initial coverages. The simulated TPD set is compared to corresponding experimental data and the residual error is used as a measure of the quality of the ki-

[a)]Author to whom correspondence should be addressed. Fax: 509-376-6066. Electronic mail: bruce.kay@pnl.gov

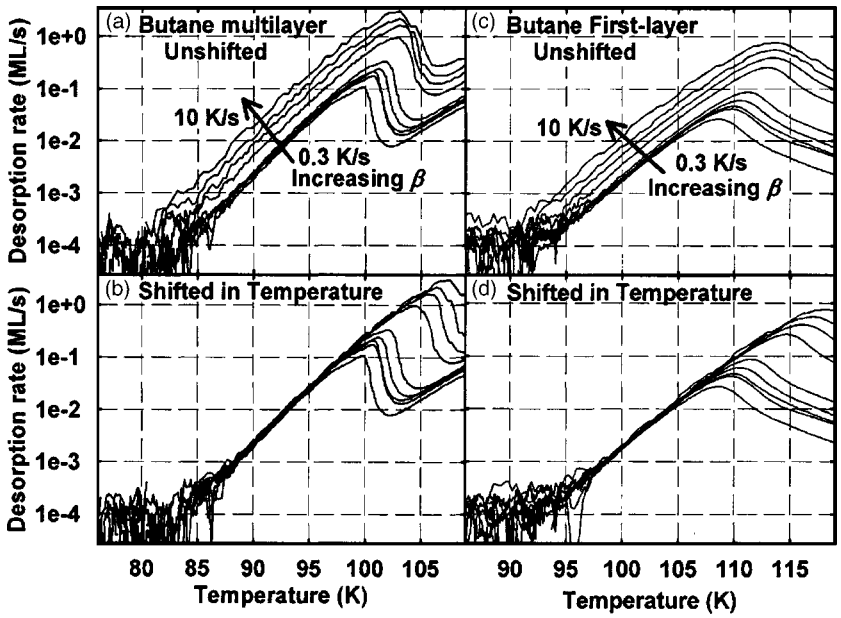

FIG. 1. Butane on MgO(100) TPD data plotted on a log scale for nine heating ramp rates β: 0.3, 0.5, 0.6, 0.7, 1.0, 3.0, 5.0, 7.0, and 10.0 K/s. Panels (a) and (b) show desorption from the multilayer of butane for an initial coverage of 2.49 ML. Panels (c) and (d) show desorption from the first layer of butane for an initial coverage of 0.42 ML. Due to temperature gradients on the sample the TPD peaks for high ramp rates appear shifted to lower temperatures, as shown in panels (a) and (c). In panel (b) we have shifted the data in panel (a) in temperature so that the leading edge of the multilayer peaks lines up. The temperature shifts of 0.3, 1.7, 2.6, 3.4, and 4.5 K were applied to the data acquired with the five highest heating rates, 1.0, 3.0, 5.0, 7.0, and 10.0 K/s, respectively. There remains a spread of about 0.5 K between the leading edges of the peaks at a desorption rate of 0.002 ML/s, which is approximately the uncertainty in the temperature shift. We show in panel (d) that the leading edge of the first-layer peak is also lined up well after this temperature shift is made.

netic parameters. The prefactor is treated as a variational parameter to minimize the difference between the experimental and simulated TPD. The present paper explains this method in detail and validates it so that it can be used as a general method for TPD analysis. This paper will also address the interactions of butane with MgO(100) and the coverage dependence of its desorption activation energy, thereby motivating an analysis which captures the coverage dependence of the desorption kinetics.

In the accompanying paper,[17] we use the analysis method presented here to study the desorption kinetics for a series of *n*-alkanes (C_NH_{2N+2}, $N=1-10$). We find that the desorption energy increases linearly with chain length, with a small *y*-intercept value. We also find that the prefactor increases by six orders of magnitude with increasing chain length, consistent with the increase in rotational entropy of the gas-phase-like transition state.

EXPERIMENT

The experimental apparatus has been described in detail elsewhere.[18] All experiments were conducted in an ultrahigh vacuum chamber with a base pressure of $\sim 1\times 10^{-10}$ Torr. High-quality MgO(100) films were produced by vapor deposition of Mg from a directional source in a background of 1×10^{-6} Torr O_2 onto a Mo(100) substrate held at 600 K. The sample is then annealed at 1000 K in the O_2 background. For film thicknesses greater than 30 layers, as employed in the present work, a sharp low-energy electron-diffraction (LEED) pattern is observed and temperature-programmed desorption (TPD) experiments demonstrate surface defect densities comparable to those obtained by UHV cleavage of MgO crystals.[18] The low electrical and thermal conductivity of magnesium oxide makes it advantageous to use a thin film of MgO rather than a cleaved bulk crystal.

The sample temperature can be controlled accurately from 20 to 2000 K by attachment to closed-cycle He cryostat cooling and resistive heating. The sample temperature is measured by a thermocouple spot-welded to the back of the sample. Calibration of the absolute temperature of the sample is done by multilayer desorption of N_2 and CH_4 at a moderate heating rate (0.6 K/s).[19] The multilayer desorption peak position for about 2-ML initial coverage for each molecule is referenced to previous measurements. This was simply a zero-offset correction for this sample and thermocouple mounting, assuming the proper slope of thermocouple voltage versus temperature, which had been calibrated previously for this temperature control system.

A supersonic molecular beam of the pure gas was used to deposit *n*-butane, C_4H_{10}, at a rate of 0.13 ML/s at normal incidence to the sample. The beam nozzle was held at room temperature. During deposition, the sample was held at 24 K, a temperature well below the onset of the butane multilayer desorption (see Fig. 1). There was no dissociation of the butane on the MgO surface as confirmed by Auger electron spectroscopy (AES) and by the excellent reproducibility of subsequent TPDs upon repeated doses. The reflected flux of the molecular beam was measured by a quadrupole mass spectrometer (QMS) in a line-of-sight position and was used as a measure of the butane uptake by the sample and as a verification that molecular-beam fluxes were the same from experiment to experiment.

TPD experiments were conducted by heating the sample at a constant rate and measuring the desorption rate of butane

by QMS ($m/e=43$) in a line-of-sight position at an acquisition rate of 22 Hz. The quantitative analysis of desorption rates here assumes that the angular distribution of desorbing alkanes is independent of coverage and temperature. This was verified by measuring TPD using mass spectrometers in both line-of-sight and background positions. Any errors associated with this assumption were minimized by locating the QMS at about 30° from sample normal, near the so-called magic angle ($\sim 35°$).[20] TPD measurements were made at a heating rate of 0.6 K/s for 29 initial coverages of butane ranging from 0 to 3.70 ML. Every fourth experiment was conducted with the same dose time (10-s dose, 1.13 ML) to check that the deposition rate from the molecular beam was constant and to watch for slight drift in the temperature measurement. The deposition rate varied by no more than 3% and showed no systematic drift. By comparing the desorption peak leading edges of this control set we concluded that the calibration of the temperature measurement varied by less than 0.25 K with no systematic trend.

Effect of temperature gradient on TPD line shape

We also made TPD measurements at 11 other temperature ramp rates in the range of 0.05–10 K/s, each at seven initial coverages in the range of 0.10–2.49 ML. We found the TPD signal-to-noise ratio at the lowest heating rates (0.05–0.1 K/s) unacceptable for our detailed analysis. Although the absolute temperature of the sample had been calibrated as described above (at 0.6 K/s), it was found that a further additive correction to the thermocouple temperature was needed for heating rates of 1.0 K/s and higher in order for the thermocouple to reflect the average desorption temperature in each case. The thermocouple reading lagged behind the average desorption temperature by 0.3 to 4.5 K at heating rates of 1.0–10 K/s due to the fast heating and finite thermal conductivity of the sample. This calibration was determined by monitoring the leading edges of the desorption peaks of the butane multilayer at several heating rates.

In Fig. 1(a), we have plotted butane multilayer desorption peaks for 2.49-ML initial coverage on a log scale. The leading edges of these peaks, acquired at various heating ramp rates, do not coincide as they should. As we discuss below, the desorption rate is a single-valued function of coverage and temperature. The leading edges of the TPD peaks for these various heating rates represent the limit where negligible desorption has occurred (each experiment has same initial butane coverage) and so we expect the peaks to be aligned in that region (i.e., the desorption rate at a given temperature to be independent of heating rate). The line shape of this multilayer desorption peak is characteristic of coverage-independent (zero-order) desorption kinetics in which case the leading edge should line up until near the peak maximum. We observe that for the larger ramp rates (1.0–10.0 K/s) there is a noticeable temperature shift in the data due to temperature gradients on the sample. In Fig. 1(b), the temperature axis was shifted to align this edge with that observed for a heating rate of 0.6 K/s, at which rate we had done the absolute temperature calibration described above. The applied shifts were 0.3, 1.7, 2.6, 3.4, and 4.5 K for the heating rates of 1.0, 3.0, 5.0, 7.0, and 10.0 K/s, respectively. After correcting the temperature in this way, the leading edges of the multilayer desorption peaks line up to within 0.5 K at a desorption rate of 0.002 ML/s and the positions of the peak maxima increase monotonically with increasing heating ramp rate.

Figure 1(c) is a log plot of the first-layer desorption peaks (at the same set of heating rates) for a submonolayer coverage (0.42 ML) of butane. Without the above-mentioned correction, the leading edges of these peaks for the various heating ramp rates do not coincide. Figure 1(d) shows these data corrected using the same temperature corrections applied to the multilayer peak in Fig. 1(b). We see that this correction aligns the leading edges of the first-layer peak in the limit where the coverage on the surface is approximately equal to the initial coverage (each curve has the same initial coverage). We note that the dynamic range of these data is three to four orders of magnitude above the background noise, making resolution of the leading edges in the limit $\theta \approx \theta_0$ possible.

Alignment of the leading edges of the multilayer peaks rather than the first-layer peaks was used to determine the temperature corrections needed for each heating rate because the first-layer peak leading edges may also be affected by intermolecular interactions which would prevent the adsorbed molecules from maintaining a dynamic equilibrium on the surface (i.e., inhomogeneous surface coverage of adsorbates). This effect was proven to be negligible in the present case, as the leading edges of the first-layer peaks coincide to within 0.5 K after applying the temperature correction derived from the multilayer peaks [Fig. 1(d)].

This heating rate-dependent temperature correction is due to a temperature gradient which will exist on any sample of finite thermal conductivity with nonuniform heat input. In our experiment, heat transfer to the disk-shaped sample occurs at the two contacts to the heating wires located on opposite edges of the back of the sample. The temperature is read at another point near the perimeter of the sample, but away from the heat inputs. The gradient across the sampled area depends on a number of factors: (a) the thermal conductivity of the sample, (b) the relative locations of the heat input to the sample and the thermocouple, and (c) the heating ramp rate. The temperature gradient leads to a convolved TPD peak due to the different desorption rates from various regions on the sample which are at different temperatures. We have modeled the effect of temperature gradient on TPD using a simple finite element calculation based on the geometry of our sample. At heating rates in the range of 1.0–10.0 K/s, the peak shape does not change significantly but there is a shift in the apparent TPD peak position, due to the difference between the average sample temperature and the temperature measured by the thermocouple. The effect at higher heating rates is a significant distortion (broadening) of the TPD peak and so we did not conduct experiments at heating rates greater than 10 K/s.

The temperature shift required to align the leading edges of the multilayer peaks in Fig. 1(b) increases linearly with heating rate and is fit well by a line with a y intercept of zero and a slope of 0.49 s. A calculation done by Carter and An-

ton shows that a characteristic time for temperature gradients on a disk-shaped sample of radius r is well estimated by calculating these gradients in a one-dimensional rod[21] of half-length $l=r$. The thermal conductivity κ, density ρ, and specific heat c_p of the sample material (1.38 W/cm K, 10.2 g/cm^3, and 0.251 J/g K, respectively for Mo)[22] are used to calculate the thermal diffusivity of the substrate. The characteristic time can be calculated as

$$t_c = \frac{l^2}{\alpha} = \frac{l^2 \rho c_p}{\kappa}. \quad (1)$$

A detailed analysis of the thermal conductivity of our sample is beyond the scope of this paper, however, using Carter's model with the thermal properties of molybdenum, we estimate the time constant to be on the order of $t_c=0.5$ s for a molybdenum rod with half-length $l=5$ mm, corresponding to the radius of our disk sample. This time constant can be used to estimate the magnitude of the temperature gradient in the sample where it is assumed that the two ends of the rod are at the same temperature. The gradients predicted by Carter's model[21] are of magnitude $\Delta T=\beta t_c/2$, where β is the heating rate. The gradients on our sample are estimated to be 0.075–2.5 K for ramp rates of 0.3–10 K/s, comparable to the temperature shifts we observe (within the factor of order one that Carter quotes for the accuracy of his model).[21]

We will discuss below our method for analyzing the TPD results as well as two well-known methods, the Redhead peak temperature analysis[23–25] and the complete analysis.[26,27] We note here that the temperature correction described above is critical for each of these analysis techniques to provide reliable results when examining how the TPD peak shifts as a function of heating rate. We do not elaborate on this point as it has been discussed previously regarding the complete analysis technique.[21] The data presented and analyzed in the following discussion have all been temperature corrected according to the procedure outlined in this section.

RESULTS AND DISCUSSION

TPD with varying initial coverage

The TPD data for a series of initial coverages of butane on MgO(100) are plotted in Fig. 2. The 16 initial coverages of butane are in the range of 0–1.76 ML. Thirteen other initial coverages from 0.24 to 3.70 ML were also studied, but are not shown for clarity of presentation. There are two prominent, well-resolved desorption peaks for butane: desorption from the multilayer (99 K) and desorption from the first layer (110 K) of butane.

The butane multilayer desorption peak has a shape characteristic of zero-order (coverage-independent) desorption kinetics, where the leading edges for various initial coverages line up until their maxima, at which the multilayer is exhausted and the desorption rate drops sharply. With increasing initial coverage the peak maximum increases in intensity and shifts to higher temperature. For a 2.0-ML initial coverage and a ramp rate of 0.6 K/s the peak maximum is positioned at approximately 99 K. The second and higher layers were not resolved in this multilayer desorption peak.

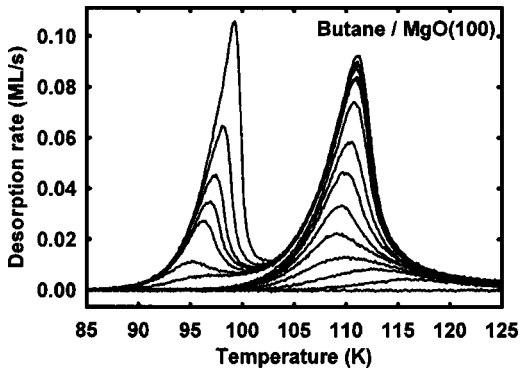

FIG. 2. Representative TPD spectra of butane/MgO(100) at a heating rate of 0.6 K/s for 16 initial coverages in the range of 0–1.76 ML: 0.00, 0.10, 0.19, 0.28, 0.42, 0.51, 0.66, 0.76, 0.88, 1.05, 1.13, 1.21, 1.31, 1.38, 1.52, and 1.76 ML. Two desorption peaks are resolved, multilayer (99 K) and first-layer (110 K) desorption, as well as a high-temperature tail on the first-layer peak due to desorption from defect sites on the surface. For clarity of presentation, 13 other initial coverages (0.24–3.70 ML) are not shown.

The desorption peak from the first layer of butane on the surface is centered at 110 K. It is characteristic of desorption kinetics that are first order in butane coverage (i.e., nearly the same peak position for any initial coverage). There is a slight (2 K) shift of the first-layer peak to higher temperature with increasing coverage in the range of 0.4–1.0 ML, indicating an attractive interaction between the adsorbed butane molecules. One monolayer (ML) is defined to be the number of molecules per unit area required to saturate the first-layer peak. The initial coverage was determined for each spectrum by integration of the desorption rate with respect to time and normalizing the integrated area to the area of the saturated first-layer peak.

Also noticeable on this first-layer peak is a high-temperature tail. It is clear from the coverage evolution of Fig. 2 that this tail is *not* due to a limitation in pumping speed (>5000 L/s in this chamber), as the tail saturates in height at relatively low initial coverage and does not increase in size proportional to the first-layer peak. At the lowest initial coverages shown in Fig. 2 it becomes apparent that this tail is a smaller desorption peak which we interpret to be due to the desorption of butane from defect sites on the surface. The saturation of this peak before the filling of the first-layer peak indicates that the butane molecules have sufficient mobility on the MgO(100) surface to find the most energetically favorable adsorption site. The area of this "defect" peak is difficult to deconvolute from the peak at 110 K, but it appears to have saturated at an initial coverage of ~0.2 ML in Fig. 2. We compare this to previous desorption studies of D_2O (Ref. 28) and CO (Ref. 29) from single-crystal MgO(100) surfaces which show a similar high-temperature tail. We estimate that the area of the tail in those studies corresponds to approximately 0.15 ML of adsorbate. It has been remarked previously that the amount of the adsorbate that is influenced by defect sites cannot be equated to the density of surface defects, as the binding of an adsorbate molecule in the vicinity of a defect-bound adsorbate molecule may also be influenced by the defect or several adsorbate molecules could be stabilized by one defect.[18]

The presence of these defect sites (of which there may

be several species with unique binding energies) as well as the shift in the first-layer peak due to intermolecular attraction make it clear that the effective desorption energy barrier must have some dependence on the coverage of butane. At low butane coverages it represents a convolution of the activation energies for desorption from the various defect sites with those for desorption from MgO terrace sites. The effect of this convolution on the desorption energy decreases with increasing coverage. Additionally, the energy shows some increase with coverage due to the adsorbate–adsorbate attraction. Therefore, an analysis of these data to yield coverage-dependent kinetic parameters is necessary to accurately characterize this system.

From the high-quality TPD data presented here we are able to extract the coverage dependence of the desorption kinetics using an analysis which has been presented previously[18] and which we will elaborate and develop further here. The coverage of butane θ on the surface at any given temperature T is calculated by integrating the desorption rate signal with respect to temperature (time) from T to the limit $T \rightarrow \infty$, i.e.,

$$\theta(T) = \frac{1}{\beta}\int_{T}^{\infty} \frac{d\theta}{dT'} dT', \tag{2}$$

where $\lim_{T\rightarrow\infty} \theta(T) = 0$ and $\beta = dT/dt$.

Each TPD spectrum provides the desorption rate $r(\theta, T)$ versus time for a given initial coverage and heating rate. The desorption rate is a single-valued function of temperature and coverage. The Polanyi–Wigner equation gives the desorption rate r as a function of θ and T:

$$r(\theta,T) = -\frac{d\theta}{dt}(\theta,T) = \nu_n(\theta,T) e^{-E_d(\theta)/k_B T}\theta^n, \tag{3}$$

where k_B is the Boltzmann constant, n is the order of desorption, E_d is the activation energy for desorption, and ν is the preexponential factor. By mathematical inversion, the coverage-dependent desorption activation energy $E_d(\theta)$ can be obtained from the Polanyi–Wigner equation

$$E_d(\theta) = -k_B T \ln\left[-\frac{d\theta/dt}{\nu\theta}\right]. \tag{4}$$

Here we assumed that desorption is a first-order process ($n = 1$) and that ν does not vary with coverage or temperature. The latter assumption is somewhat arbitrary as the coupling of $\nu(\theta, T)$ and $E_d(\theta)$ would allow the coverage dependence to be captured mathematically by either variable. Physically, a variation of the prefactor with coverage would occur if the partition function of the adsorbate varied significantly in different adsorption sites on the surface or due to the adsorbate–adsorbate interactions. The energy will change with coverage as various adsorption sites (e.g., point defects, step defects, kink defects, terrace sites, etc.) will have different coordination numbers of the substrate ions to the adsorbate leading to different strengths of the physisorption interaction. Also it is clear that van der Waals forces (or any other interactions) between the adsorbates will lead to changes in the desorption activation energy with coverage. Therefore, the coverage dependence of the energy term is generally expected and its interpretation in terms of energy variations due to various adsorption sites and adsorbate–adsorbate interactions is well established.

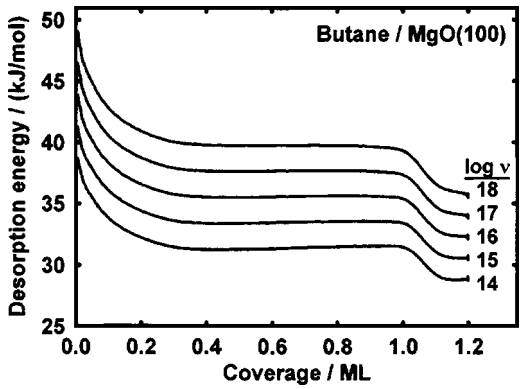

FIG. 3. Desorption energy vs butane coverage for desorption of butane from the MgO(100) surface for five different initial estimates for the prefactor: 10^{14}, 10^{15}, 10^{16}, 10^{17}, and 10^{18} s^{-1}. The desorption energy is calculated from a single measured TPD spectrum ($\theta_0 = 1.2$ ML, $\beta = 0.6$ K/s) by inversion of the Polanyi–Wigner equation [Eq. (4)], assuming a coverage-independent value for prefactor, as described in the text.

Figure 3 shows the coverage-dependent desorption energy of butane from the MgO(100) surface for each of five assumed values of the prefactor ($\nu = 10^{14}$, 10^{15}, 10^{16}, 10^{17}, 10^{18} s^{-1}). Each energy curve in Fig. 3 was calculated using Eq. (4) and a TPD spectrum of 1.2-ML initial coverage of butane with a heating rate of 0.6 K/s. The general behavior (shape) of the coverage-dependent energy curve is the same for each choice of ν. At low coverages, the energy is high, corresponding to the binding of butane molecules at the point and step defects on the oxide surface. The energy decreases as the coverage increases to about 0.3 ML and the butane molecules begin to fill the MgO terraces. In the coverage range of 0.3–0.8 ML the desorption energy appears to be nearly constant. However, there is a gradual rise ($<1\%$) of the desorption energy with increasing coverage in this region due to attractive interactions between the molecules. This corresponds to the slight shift in the desorption peak toward higher temperature with increasing initial coverage. As the coverage increases above 1.0 ML, the desorption energy again decreases as the molecules compress the first layer and begin to fill the second layer.[30] These characteristics of the desorption energy curve are independent of ν. While the general shape of the curves is similar, it is clear that the absolute energy shifts to higher values of E_d with increasing ν.

For purposes of comparison, we show in Fig. 4 the experimental TPD data (diamonds) for four initial coverages (0.42, 0.58, 0.84, and 1.20 ML). The lines in Fig. 4 are simulations of the experimental TPD data using the energy result shown in Fig. 3. Each line style corresponds to a different assumed value for the prefactor, each varying by a factor of 10. The highest initial coverage data set shown in Fig. 4 (1.2 ML) was used to obtain the desorption energy values in Fig. 3 for each of the five prefactors. The simulated TPD spectra for that initial coverage fit perfectly for any prefactor value, since these experimental data were mathematically inverted to yield the coverage-dependent desorption energy. For any choice of ν, one can choose a desorption

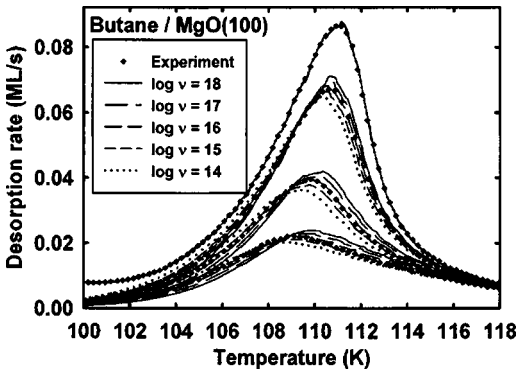

FIG. 4. Experimental TPD data (diamonds) for butane/MgO(100) at 0.6 K/s and four initial coverages 0.42, 0.58, 0.84, and 1.20 ML. Data points for the highest initial coverage were inverted via the Polanyi–Wigner equation to construct the coverage-dependent energy curves shown in Fig. 3 for five initial estimates for the prefactor. Simulations are also shown for the four initial coverages using those five energy curves and prefactor values: 10^{14} s^{-1} (dotted lines), 10^{15} s^{-1} (short dashed lines), 10^{16} s^{-1} (medium dashed lines), 10^{17} s^{-1} (long dashed lines), and 10^{18} s^{-1} (solid lines). The best match to the experimental data points is the set of simulations based on a prefactor of 10^{16} s^{-1}.

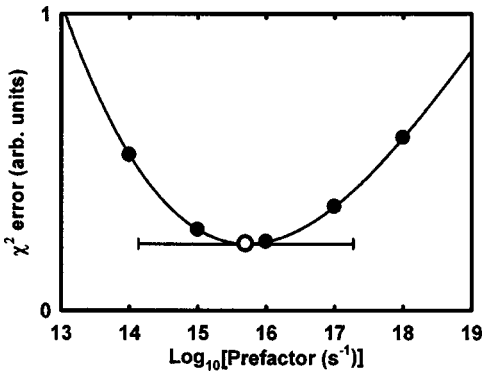

FIG. 5. The χ^2 error between the simulations and experiments shown in Fig. 4 as a function of the prefactor assumed in the inversion analysis for each prefactor used in Figs. 3 and 4 (black circles). The solid line in this figure is a fourth-order polynomial fit, which shows that the minimum error occurs at $10^{15.7}$ s^{-1} (open circle). We estimate the error in log(prefactor) to be better than ±10% (error bar).

energy value that will yield a given desorption rate and therefore construct a function $E_d(\theta)$ which will perfectly simulate the same TPD data back again. Other constraints are necessary to determine an accurate value of the prefactor. We have developed a methodology which yields a reliable value for the prefactor (within the assumption that it does not vary with coverage) by using the calculated $E_d(\theta)$ to simulate a set of TPD spectra at different initial coverages.

We see that the quality of the fit for the three lower initial coverages in Fig. 4 depends strongly on the choice of prefactor. The correct combination of ν and $E_d(\theta)$ should be able to accurately reproduce TPDs for any set of initial coverages. Of the five prefactors used to generate the simulations in Fig. 4, it appears that 10^{16} s^{-1} is the best choice. Simulations based on lower prefactors show less agreement with the experimental data as the desorption rate is too high on the leading edge of the peak then too low on the trailing edge of the peak, causing the desorption peak to be smaller in height and to be centered at a lower temperature compared to the experimental data. Higher choices of prefactor show the opposite trend: desorption rate is too low on the leading edge and too high on the trailing edge, causing the peak to be too tall and shifted to higher temperature. Thus, by treating the prefactor as a variational parameter to optimize the fit between experimental and simulated TPDs, we can find the prefactor that best matches the kinetics of the desorption process.

The quality of the fit of the simulation to the experimental data is quantified by calculating a χ^2 error between the simulated and experimental TPD curves for five initial coverages (not including the inverted experimental set), only three of which are shown in Fig. 4 for clarity of presentation. The χ^2 error is defined as the sum of the squares of the residuals of the simulation compared to the experiment at each data point on the experimental TPD spectrum. As shown in Fig. 5, the magnitude of the χ^2 error has a well-defined minimum with respect to the assumed value of prefactor. These error values have been fitted with a polynomial function (solid line in Fig. 5) and the minimum of that function is indicated by the open circle at $\nu=10^{15.7}$ s^{-1}, very close to the best "fit by eye" one would obtain from Fig. 4. The reason this value exceeds 10^{13} s^{-1} is explained in the accompanying paper.[17] This value which minimizes the χ^2 error was found to be statistically accurate to within ±0.1 in log ν, as evidenced by the larger error for $\nu=10^{15.6}$ and $10^{15.8}$ s^{-1}. However, we estimate a larger prefactor error based on potential systematic errors associated with the thermocouple and QMS measurements, but still certainly less than ±10% in log ν. Using the best-fit value for the prefactor, we calculate the coverage-dependent desorption energy of butane from MgO(100), which has a value of 34.9±3.4 kJ/mol at 0.5-ML coverage. The stated error here corresponds to the 10% uncertainty in the log of the prefactor.

This result, the "best-fit" prefactor and corresponding coverage-dependent desorption energy, is used to simulate a set of TPDs for five initial coverages, shown as solid lines in Fig. 6. The solid points in Fig. 6 are experimental data for initial coverages of 0.19, 0.42, 0.58, 0.84, and 1.00 ML. The simulations capture the peak position (desorption tempera-

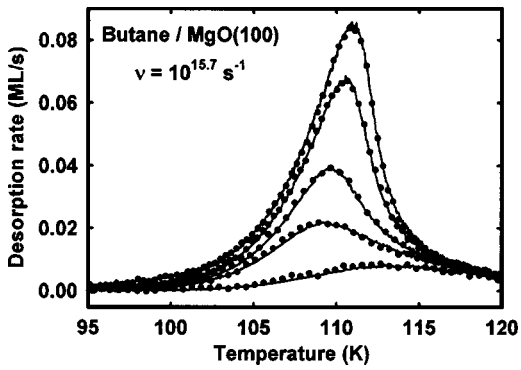

FIG. 6. Representative butane/MgO(100) TPD experiment (points) and corresponding simulations (lines) at 0.6 K/s for five initial coverages, 0.19, 0.42, 0.58, 0.84, and 1.00 ML. Simulations are based on the coverage-dependent desorption energy calculated from the best-fit prefactor, $10^{15.7}$ s^{-1} and inversion of the $\theta_0=1.2$-ML TPD spectrum (shown in Fig. 4). Not all data points are shown for clarity of presentation.

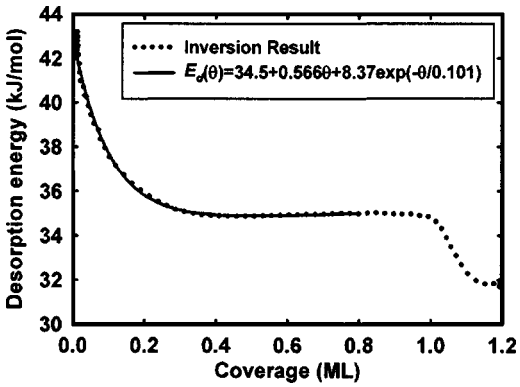

FIG. 7. Desorption energy vs coverage for butane TPD from MgO(100). Energy calculated by inversion method described in the text (dotted line) from TPD data at 0.6 K/s, assuming a coverage-independent prefactor at its best-fit value of $10^{15.7}$ s^{-1}. The solid line is an analytic equation for the desorption energy in units of kJ/mol (see figure legend) which has four free parameters that have been adjusted to provide the best fit in the coverage range of 0–0.8 ML.

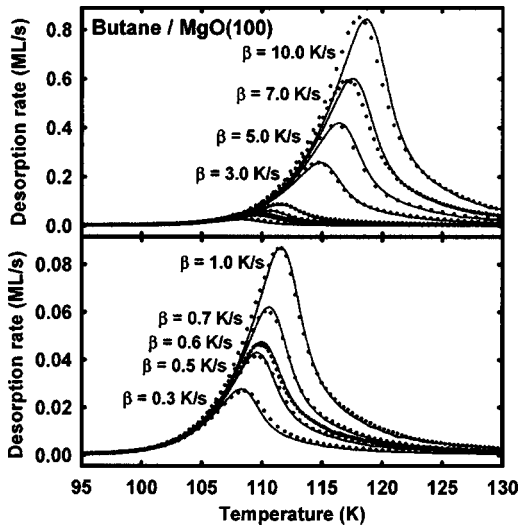

FIG. 8. Comparison of experimental TPD data (dots) to simulations based on the inversion analysis ($\nu=10^{15.7}$ s^{-1}, solid lines) for nine heating ramp rates of 0.3–10 K/s. The initial coverage was 0.73 ML. The experimental data have been shifted in temperature to line up leading edges (no shifts applied for curves <0.6 K/s). The bottom panel is scaled to show greater detail of the low heating rate peaks in the top panel. Only every eighth data point is shown for all experimental curves, except 7 and 10 K/s. Each experimental curve was smoothed except 5, 7, and 10 K/s.

ture) of the experiment and they also reproduce very well the shape of the desorption curve, including the subtle shifts in temperature due to the adsorbate–adsorbate interactions as well as the high-temperature shoulder due to the influence of the defect states on the desorption kinetics of butane.

To a good approximation, the coverage dependence of the desorption energy can be represented well over the coverage range of 0–0.8 ML by the analytic function

$$E_d(\theta) = E_0 + \gamma\theta + E_{\text{def}} \exp(-\theta/\theta_{\text{def}}) = 34.5 + 0.566\theta + 8.37 \exp(-\theta/0.101), \quad (5)$$

where all energies are in kJ/mol. This function has been constructed to express the general behavior of the desorption energy with respect to coverage without unnecessary complexity. This function is plotted in Fig. 7 along with the result of the inversion analysis. We see that it matches the inversion result well and we note that using this analytic result to simulate TPD (not shown here) shows a very good fit to the experimental results. The first term E_0 represents the desorption energy one would obtain by extrapolating the linear region of the coverage-dependent energy curve back to the limit of zero coverage. This is the number that could most readily be interpreted as the activation energy for desorption of an isolated butane molecule from a MgO(100) terrace site (i.e., in the absence of defect sites and adsorbate–adsorbate interactions). The factor γ is the increase in desorption energy per ML increase in coverage. The positive sign of this number indicates an attractive interaction between the butane molecules on the MgO(100) surface. This "interaction" term in our empirical fit is weak, accounting for only 1.3% of the desorption activation energy at 0.8-ML coverage. The value of γ is also much, much smaller than the bulk sublimation (cohesive) energy of butane, suggesting that this attraction is not simply equal to the van der Waals attraction between butane molecules, unperturbed by the substrate. Clearly, there is an influence of the substrate on adsorbate spacing and polarization. In the limit of strong interadsorbate attractions, the adsorbates form two-dimensional (2D) islands in equilibrium with a 2D gas,[31] leading to zero-order desorption kinetics and a much, much smaller value of γ than the true adsorbate–adsorbate attraction.[32]

E_{def} is the energy difference between E_0 and the measured desorption energy at zero coverage $E_d(0)$ and is related to the difference between the adsorption energy of a butane molecule adsorbed on a MgO terrace site compared to one adsorbed at a defect site. The factor θ_{def} corresponds to the rate at which the influence of defect sites on the energy result decays with increasing coverage. It is related to the density (coverage) of defect sites on the oxide surface as well as to the degree to which defect sites influence the adsorption of molecules that are near molecules adsorbed at defects. This term may give a more reliable insight into the actual density of defects on the surface rather than looking at the area under the defect shoulder in the TPD spectrum, but we do not wish to overinterpret this empirical fit function.

TPD with varying heating ramp rate

Variation of the heating ramp rate over a set of TPD experiments allows one to extract more information about the desorption kinetics by recording the desorption rate for a given coverage at several different values of temperature. TPD experiments were conducted using a set of eleven different heating ramp rates (0.05, 0.07, 0.1, 0.3, 0.5, 0.7, 1.0, 3.0, 5.0, 7.0, and 10.0 K/s) and seven initial coverages (0.10, 0.22, 0.44, 0.73, 0.91, 1.20, and 2.49 ML).

Experimental data points for butane desorption (0.73-ML initial coverage) from MgO at heating rates of 0.3, 0.5, 0.6, 0.7, 1.0, 3.0, 5.0, 7.0, and 10.0 K/s are plotted in two panels in Fig. 8 and have been temperature corrected, as discussed in the Experiment Section. The difference in the lower panel from the upper is only that the *y* axis has been rescaled to show more detail in the desorption peak for the five lowest heating rates. We have also simulated TPD at

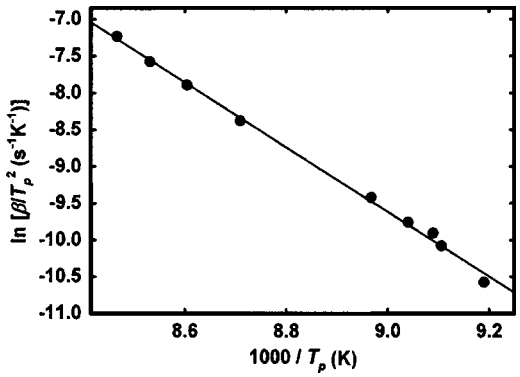

FIG. 9. Redhead heating rate/desorption peak temperature analysis for nine TPD experiments from 0.3 to 10 K/s and an initial coverage of 0.42 ML. The solid line is a linear fit from which we obtain a desorption energy of 36.6 ± 0.7 kJ/mol and a prefactor of $10^{16.7\pm0.3}$ s^{-1} (stated error is statistical error in linear regression). We compare these results to the result from the inversion analysis, evaluated at 0.5-ML coverage: $E_d=34.9\pm3.4$ kJ/mol and $\nu=10^{15.7\pm1.6}$ s^{-1}.

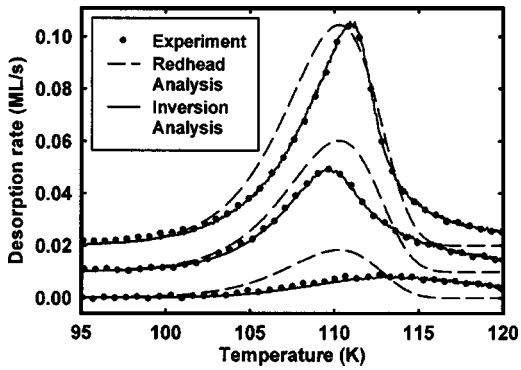

FIG. 10. Comparison of TPD for butane at three initial coverages (0.19, 0.58, 1.00 ML). The circles are experimental data, the solid lines are simulations based on the result of the inversion analysis, and the dashed lines are simulations based on the result of the Redhead heating rate analysis. Only every 12th point of experimental data is shown and each initial coverage is offset by 0.01 ML/s along the vertical axis for clarity of presentation.

these heating rates using the desorption energy versus coverage curve discussed previously (Fig. 7) which was calculated by inversion of a TPD taken at 0.6 K/s (highest peak in Fig. 4), using the best-fit prefactor value of $\nu=10^{15.7}$ s^{-1}. These simulations are plotted as solid lines in Fig. 8. The leading edges of the simulated curves line up perfectly as they are simulated without temperature gradients. We see that the agreement between simulation and experiment is excellent for the choice of $\nu=10^{15.7}$ s^{-1}, demonstrating the robustness of our inversion method over a wide range of heating ramp rates. The simulation matches experiment best at ramp rates of 0.5–3.0 K/s (i.e., near the heating rate of the inverted spectrum, 0.6 K/s). In Fig. 8, we see that at higher ramp rates the simulation misses the experimental data by about 0.5 K, an error of less than 0.5% in temperature or desorption energy. The desorption peak shape is reproduced well by the simulation, even at high ramp rates. The high-temperature tail due to desorption from defect states is matched well by the simulation and scales appropriately with heating rate.

Redhead heating rate analysis

Using the set of TPD data at various heating rates, the desorption energy and prefactor information can be extracted from the set of desorption peak temperatures, using the Redhead method.[23–25] This method has been used in several previous studies of the desorption of alkanes, C_NH_{2N+2}.[8,11,13,15] In this method, the Polanyi–Wigner equation is evaluated at the desorption peak temperature and rearranged to make an Arrhenius form for the peak desorption temperature, T_p at different heating rates β,

$$\ln\left(\frac{\beta}{T_p^2}\right) = -\ln\left(\frac{E_d}{k_B\nu}\right) - \frac{E_d}{k_B}\frac{1}{T_P}. \tag{6}$$

Implicit in this analysis is the assumption of coverage-independent desorption-kinetics parameters (ν and E_d). We have compiled the peak temperatures T_p for the TPD data shown in Fig. 8 and we plot $\ln(\beta/T_p^2)$ versus $1/T_p$ in Fig. 9. We see that these points fit well to a line (shown in Fig. 9). The slope of the linear fit in Fig. 9 corresponds to a desorption energy of 36.6 ± 0.7 kJ/mol. The y intercept of that line corresponds to a prefactor value of $10^{16.7\pm0.3}$ s^{-1}. The errors quoted here correspond to the statistical error in the linear regression and do not account for experimental error in the T_p values, thus they seem much smaller than the maximum error values quoted for the inversion analysis. These results of the Redhead method are in agreement with the results of the inversion analysis, $\nu=10^{15.7\pm1.6}$ s^{-1} and $E_d(\theta=0.5\ \mathrm{ML})=34.9\pm3.4$ kJ/mol, within the error of the two analysis methods. We can also compare the Redhead method results to previous TPD studies of butane on $Al_2O_3(0001)$ analyzed using the same method. On that surface, a desorption energy of 35.1 ± 5.9 kJ/mol with a prefactor of $10^{10.6\pm2.5}$ s^{-1} was measured.[13]

We have used the result from the Redhead peak temperature method to simulate TPD experiments at several initial coverages, and have plotted these in Fig. 10. The solid points represent the experimental data and the dashed lines are simulations based on the Redhead analysis approach. For comparison, we also plot the simulations from our inversion analysis as solid lines. We see that the Redhead method matches the desorption peak temperature for the higher initial coverages well, but that its ideal first-order peak shape does not match the experimental peak shape. Also, this method completely misses the small peak (tail) due to desorption from defect states, since it assumes coverage-independent desorption-kinetics parameters. The simulation based on the inversion analysis (solid lines) contains coverage-dependent parameters and hence matches the data very well.

Complete analysis

A common analysis method which yields coverage-dependent values for both prefactor and desorption energy is referred to as complete analysis.[26,27] This technique consists of measuring TPD over a wide range of coverages and/or heating ramp rates to allow measurement of $d\theta/dt(T,\theta)$ for various combinations of θ and T. From these data, isosteric (constant coverage) Arrhenius lines of $\ln[d\theta/dt(T,\theta)]$ versus

$1/T$ are constructed and fit to lines. Then the desorption energy and prefactor can be calculated for discrete coverages corresponding to each isostere.[21] A significant disadvantage to this complete analysis approach is that kinetic parameters are obtained only at discrete coverage values, which may make it difficult to accurately describe the desorption kinetics if these parameters vary rapidly in coverage, as in the present case. The inversion analysis that we have described here calculates a desorption energy value for each point on the TPD spectrum.

We have carried out this complete analysis on our data and obtained results that are generally in good agreement with the inversion analysis result. The TPD points lined up well for isosteres in the range of 0.4–0.9 ML. In that range, the prefactor and desorption energy show little coverage dependence, varying by less than 2%, and have values of $\nu = 10^{16.4}$ s^{-1} and $E_d = 36.4$ kJ/mol. For coverages less than 0.4 ML, the isosteric plots of desorption rate from different initial coverage sets of TPD did not fall on the same line and so there is a large statistical uncertainty in the resulting kinetic parameters (e.g., up to ±10% in E_d). The complete analysis provides coverage-dependent energy and prefactor information at discrete coverages in the range of 0.4–0.9 ML.

However, we note that in order to obtain such good results with the complete analysis, it was necessary first to correct high heating rate data for temperature gradients on the sample, as described in the Experiment Section. Failure to correct for such gradients would lead to spurious results. This represents a significant limitation on the experimental range over which the heating rate can be varied. It is instructive to note that our inversion-optimization analysis method obtained coverage-dependent desorption-kinetics parameters from a single heating rate. We demonstrated that these analysis results were of sufficient quality to accurately simulate experimental TPD spectra at a wide range of initial coverages and heating ramp rates. We conclude that this inversion-optimization method produces accurate coverage-dependent desorption-kinetics parameters using data obtained at a single heating rate.

SUMMARY

We have conducted temperature-programmed desorption experiments to obtain coverage-dependent kinetics parameters for the desorption of *n*-butane from the MgO(100) surface. We invert the TPD data to obtain desorption energy versus coverage information for an assumed value of the prefactor and show that the choice of prefactor strongly affects the quality of simulated TPD. By optimizing the match of the TPD simulation to data, we obtain a best-fit prefactor and coverage-dependent desorption energy which can be used to accurately simulate TPD spectra over a wide range of initial coverages and heating rates. The inversion-optimization method gives better results than the Redhead heating rate analysis and has advantages over the complete analysis. In the next article, we employ this methodology to study the chain length dependence of desorption kinetic parameters over a range of small alkane molecules.[17]

ACKNOWLEDGMENTS

Two of the authors (B.D.K. and Z.D.) funded by the U.S. Department of Energy Office of Basic Energy Sciences (OBES) Chemical Sciences and Materials Sciences Divisions. One of the authors (C.T.C.) acknowledges support by the OBES Chemical Sciences Division. Another author (S.L.T.) supported by a graduate student fellowship award from the University of Washington/Pacific Northwest National Laboratory (PNNL) Joint Institute for Nanoscience and acknowledges participation in PNNL's Interfacial and Condensed Phase Chemical Physics Summer Research Institute. All of the experimental work was performed in the Environmental Molecular Sciences Laboratory, a national scientific user facility sponsored by the Department of Energy's Office of Biological and Environmental Research and located at PNNL. PNNL is a multiprogram National Laboratory operated for the U.S. Department of Energy by Battelle Memorial Institute under Contract No. DE-AC06-76RLO 1830.

[1] J. S. J. Hargreaves, G. J. Hutchings, R. W. Joyner, and C. J. Kiely, J. Catal. **135**, 576 (1992).
[2] J. S. J. Hargreaves, G. J. Hutchings, and R. W. Joyner, Nature (London) **348**, 428 (1990).
[3] H. J. Freund, H. Kuhlenbeck, and V. Staemmler, Rep. Prog. Phys. **59**, 283 (1996).
[4] V. E. Henrich and P. A. Cox, *The Surface Science of Metal Oxides* (Cambridge University Press, Cambridge, 1994).
[5] C. T. Campbell, Surf. Sci. Rep. **27**, 1 (1997).
[6] M. Baumer and H. J. Freund, Prog. Surf. Sci. **61**, 127 (1999).
[7] C. R. Henry, Surf. Sci. Rep. **31**, 235 (1998).
[8] R. Z. Lei, A. J. Gellman, and B. E. Koel, Surf. Sci. **554**, 125 (2004).
[9] J. F. Weaver, A. F. Carlsson, and R. J. Madix, Surf. Sci. Rep. **50**, 107 (2003).
[10] M. Salmeron and G. A. Somorjai, J. Phys. Chem. **85**, 3835 (1981).
[11] J. L. Brand, M. V. Arena, A. A. Deckert, and S. M. George, J. Chem. Phys. **92**, 5136 (1990).
[12] S. M. Wetterer, D. J. Lavrich, T. Cummings, S. L. Bernasek, and G. Scoles, J. Phys. Chem. B **102**, 9266 (1998).
[13] R. M. Slayton, C. M. Aubuchon, T. L. Camis, A. R. Noble, and N. J. Tro, J. Phys. Chem. **99**, 2151 (1995).
[14] A. J. Gellman and K. R. Paserba, J. Phys. Chem. B **106**, 13231 (2002).
[15] K. R. Paserba and A. J. Gellman, J. Chem. Phys. **115**, 6737 (2001).
[16] K. R. Paserba and A. J. Gellman, Phys. Rev. Lett. **86**, 4338 (2001).
[17] S. L. Tait, Z. Dohnálek, C. T. Campbell, and B. D. Kay, J. Chem. Phys. **122**, 164708 (2005), following paper.
[18] Z. Dohnálek, G. A. Kimmel, S. A. Joyce, P. Ayotte, R. S. Smith, and B. D. Kay, J. Phys. Chem. B **105**, 3747 (2001).
[19] H. Schlichting and D. Menzel, Rev. Sci. Instrum. **64**, 2013 (1993).
[20] S. W. Pauls and C. T. Campbell, Surf. Sci. **226**, 250 (1990).
[21] R. N. Carter and A. B. Anton, J. Vac. Sci. Technol. A **10**, 344 (1992).
[22] *CRC Handbook of Chemistry and Physics*, edited by D. R. Lide (CRC, Boca Raton, FL, 1992).
[23] P. A. Redhead, Vacuum **12**, 203 (1962).
[24] D. A. King, Surf. Sci. **47**, 384 (1975).
[25] J. L. Falconer and R. J. Madix, Surf. Sci. **48**, 393 (1975).
[26] A. M. de Jong and J. W. Niemantsverdriet, Surf. Sci. **233**, 355 (1990).
[27] J. L. Taylor and W. H. Weinberg, Surf. Sci. **78**, 259 (1978).
[28] M. J. Stirniman, C. Huang, R. S. Smith, S. A. Joyce, and B. D. Kay, J. Chem. Phys. **105**, 1295 (1996).
[29] R. Wichtendahl, M. Rodriguez-Rodrigo, U. Hartel, H. Kuhlenbeck, and H. J. Freund, Phys. Status Solidi A **173**, 93 (1999).
[30] G. A. Kimmel, M. Persson, Z. Dohnálek, and B. D. Kay, J. Chem. Phys. **119**, 6776 (2003).
[31] J. L. Daschbach, B. M. Peden, R. S. Smith, and B. D. Kay, J. Chem. Phys. **120**, 1516 (2004).
[32] S.-R. Liu, Z. Dohnálek, R. S. Smith, and B. D. Kay, J. Phys. Chem. B **108**, 3644 (2004).